Indirect determination of neutron-capture cross sections for Sm isotopes

A. Simon[1,*] and F. Naqvi[2]

[1]*Department of Physics and The Joint Institute for Nuclear Astrophysics, University of Notre Dame, Indiana 46556-5670, USA*

[2]*Department of Physics & Astrophysics, University of Delhi, Delhi 110007, India*

(Received 13 September 2019; published 28 January 2020)

Neutron-capture cross sections in the energy range of 0.01–10 MeV for ^{146,148,150,152}Sm nuclei were calculated using the γ-ray strength and level density functions extracted from the Oslo-type experiments. The uncertainties in the cross-section values were determined using a Monte Carlo method. For the ^{148,150,152}Sm isotopes, the calculated cross sections are in a good agreement with the existing experimental data and for the ^{146}Sm nucleus, an experimental (n, γ) cross section is reported for the first time. The results are compared with the ENDF, EAF, and TENDL evaluations. Maxwellian-averaged cross sections were also calculated using the same input γSF and LD functions.

DOI: 10.1103/PhysRevC.101.014619

I. INTRODUCTION

Neutron-capture reactions play a critical role in a variety of applications including nuclear astrophysics, nuclear energy, and national security. The astrophysical *s* and *r* processes [1], which produce most of the neutron-rich heavy elements, involve multiple neutron-capture reactions (n, γ) and competing β decays on exotic nuclei. On the other hand, in the *p* process, which produces stable neutron-deficient isotopes of heavy nuclei, the initial stages of the flow are driven by the inverse photodissociation (γ, n) reactions [2]. In both cases, the astrophysical models suffer from the limited experimental measurements of the reaction cross sections. This limitation results in large uncertainties in the predicted final isotopic abundances and thus restricts the understanding of the details of the process to define astrophysical site.

Direct measurements of (n, γ) reactions pose many challenges. The nuclei of interest are short lived and cannot be made into targets for neutron-capture cross section measurements. Though some of these nuclei can be produced as beams at existing and future exotic beam facilities, using a neutron target for such studies is still not feasible. Therefore, indirect techniques are required to determine these important neutron-capture cross sections.

There are two main complementary experimental methods that allow for indirect determination of the (n, γ) reaction cross section: the surrogate method and the Oslo method. The surrogate method [3] uses charged-particle reactions, such as (p, d), to populate compound nuclear states above the neutron threshold, and observe their probability to deexcite via γ emission. Since the compound nuclear states have no memory of their production mechanism, they decay in the same manner as if they were produced via neutron capture. The successful application of the surrogate method therefore requires a good understanding of the formation of the compound nucleus in the surrogate reaction and its subsequent decay.

The Oslo method [4], requires particle-γ coincidences to identify the excitation energy of the compound nucleus and the γ-ray cascades from its deexcitation. This information is then used to extract level densities (LD) and γ-ray strength functions (γSF) from experimental data. The experimentally determined LD and γSF form inputs for statistical model calculations that yield (n, γ) reaction cross sections. Such measurements constrain the Hauser-Feshbach (HF) inputs for the nuclei that cannot be directly accessed by experiments and provide constraints on the calculated cross sections. Recently, this method was used for more exotic systems where β decay was used to populate the compound nuclear states (i.e., the β-Oslo method [5]).

The Hauser-Feshbach formalism that is applied for calculating the cross sections of (n, γ) reactions is based on an assumption that a compound nucleus is formed, thus the reaction can be described as a two-step process:

$$A + \alpha \rightarrow C^* \rightarrow B + \beta, \tag{1}$$

and that the level density of the formed compound nucleus, C^*, is sufficiency high so that the individual resonances cannot be isolated and a statistical approach can be applied. In such a case, the cross section for reaction 1 can be written as:

$$\sigma_{\alpha\beta} = \frac{\pi}{k_\alpha^2} \frac{g_\alpha \mathcal{T}_\alpha \mathcal{T}_\beta}{\sum_i \mathcal{T}_i}, \tag{2}$$

where g_α is a statistical weighting factor, k_α is the entrance channel wave number and $\mathcal{T}_\alpha$, $\mathcal{T}_\beta$, and $\sum_i \mathcal{T}_i$ denote transmission coefficients for formation of the compound nucleus via entry channel α, decay of the compound nucleus via exit channel β and the sum over transmission coefficients for all the energetically allowed decay channels, respectively. For simplicity, the spin dependence of the formula is omitted in the above example.

*anna.simon@nd.edu

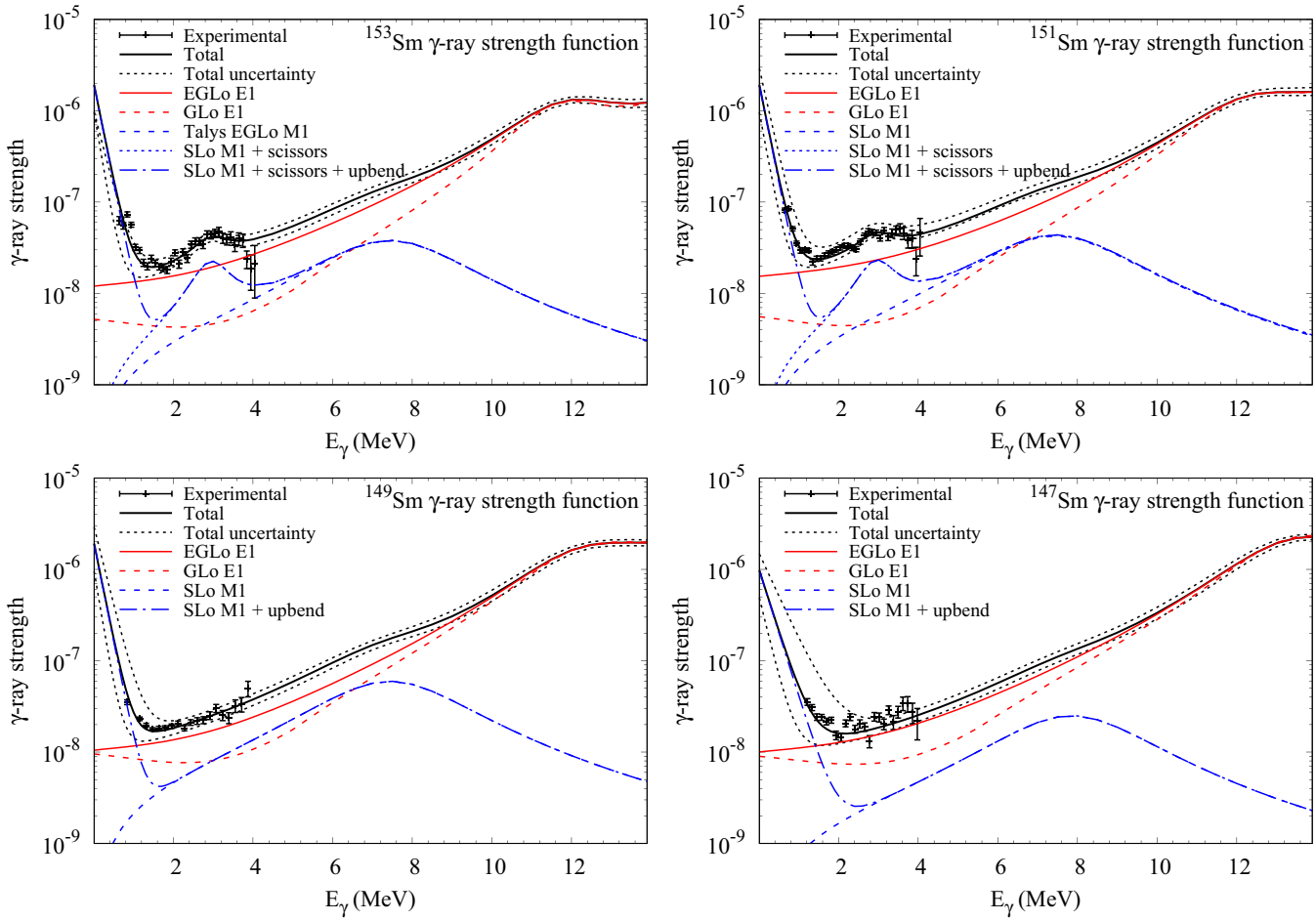

FIG. 1. γSF compared with experimental data from Refs. [11,12]. Red lines indicate the $E1$ components; blue, the $M1$; black, total γSF. The solid red line is the EGLo strength used in this work; red dashed line, the GLo available in TALYS 1.9. The black dotted lines indicate the uncertainty in the γSF based on the uncertainties of the parameters in Table I.

In case of the (n, γ) reactions, the transmission coefficients depend on the optical potential describing the reaction between the neutron and the target nuclei and on the level density of the compound nucleus. The transmission coefficient for the γ-ray deexcitation can be calculated from the γ-ray strength function as:

$$\mathcal{T}_{X\ell}(E_\gamma) = 2\pi f_{X\ell}(E_\gamma) E_\gamma^{2\ell+1}, \tag{3}$$

where $f_{X\ell}$ denotes the γ-ray strength function for the multipolarity ℓ and the electromagnetic character X.

II. HAUSER-FESHBACH CALCULATIONS

The results presented in this work were obtained using TALYS 1.9 code [6]. A microscopic optical potential of Bauge *et al.* [7] was used, however, no difference in the resulting cross section was obtained when switching to the phenomenological optical potential model that is default in TALYS. In all the calculations, proton and α breakup was disabled, as we have observed in the past that in some case they lead to incorrect cross-section values for capture reactions.

TABLE I. Parameters for GDR, spin-flip, up-bend, and the scissors mode used in this work taken from Refs. [11,12]. E, σ, and Γ denote the resonance centroid, width, and strength. η and C are defined by Eq. (11).

	Giant dipole 1 and 2 resonances							Spin-flip M1			Up-bend		Scissors resonance		
Nucleus	$E_{E1,1}$ (MeV)	$\sigma_{E1,1}$ (mb)	$\Gamma_{E1,1}$ (MeV)	$E_{E1,2}$ (MeV)	$\sigma_{E1,2}$ (mb)	$\Gamma_{E1,2}$ (MeV)	T_f (MeV)	E_{M1} (MeV)	σ_{M1} (mb)	Γ_{M1} (MeV)	C (MeV^{-3})	η (MeV^{-1})	E_{SR} (MeV)	σ_{SR} (mb)	Γ_{SR} (MeV)
^{147}Sm	13.8	200	3.8	15.5	230	5.6	0.55	8.1	2.3	4.0	$10(5)10^{-7}$	3.2(10)	–	–	–
^{149}Sm	12.9	180	3.9	15.7	230	6.5	0.47	7.7	2.6	4.0	$20(10)10^{-7}$	5.0(10)	–	–	–
^{151}Sm	12.8	160	3.5	15.9	230	5.5	0.55	7.7	3.8	4.0	$20(10)10^{-7}$	5.0(5)	3.0(3)	0.6(2)	1.1(3))
^{153}Sm	12.1	140	2.9	16.0	232	5.2	0.45	7.7	3.3	4.0	$20(10)10^{-7}$	5.0(10)	3.0(2)	0.6(1)	1.1(2)

TABLE II. Parameters used for normalizing experimentally deduced level density and γ-ray strength function taken from Refs. [11,12].

Nucleus	S_n (MeV)	$\sigma(S_n)$	D_0 (eV)	$\rho(S_n)$ (10^6 MeV^{-1})	$<\Gamma_\gamma(S_n)>$ (meV)	T_{CT} (MeV)	Shift Parameter (MeV)
^{147}Sm	6.342	6.266	252(40)	0.31(5)[a]	62(6)	0.58	−0.66
^{149}Sm	5.871	6.121	65(13)	1.04(29)	66.9(14)	0.48	−0.43
^{151}Sm	5.597	6.15	46(8)	1.66(44)	60(5)	0.51	−1.37
^{153}Sm	5.868	6.31	46(3)	1.75(36)	60(5)	0.53	−1.41

All the internal normalization routines of TALYS were disabled, so that the cross-section calculations were performed using the actual input provided. For that purpose, *ctmglobal* option was enabled and the value of the *gnorm* parameter was set to 1.0.

In all the calculations, *xseps*, *popeps*, and *transeps* parameters were set to 1.0×10^{-35} to ensure consistent round off at each step of the calculations. These parameters provide a lower limit for the calculated values of cross section, level population, and transmission coefficients, respectively. Higher values decrease computation time, but at the same time decrease the precision of the calculated cross sections.

III. γ-RAY STRENGTH FUNCTION

There are eight models of the γSF available within TALYS 1.9 that describe the shape of the $E1$ component of the γSF. Two of them are global options utilizing a Lorentzian shape:

(i) the Kopecky-Uhl generalized Lorentzian (GLo) [8],
(ii) the Brink-Axel Lorentzian (SLo) [9].

The first one is defined as:

$$f_{GLo}(\varepsilon_\gamma, T) = 8.68 \times 10^{-8}(\mathrm{mb}^{-1}\mathrm{MeV}^{-2})\sigma_0\Gamma \times \left[\frac{\varepsilon_\gamma \Gamma(\varepsilon_\gamma)}{\left(\varepsilon_\gamma^2 - E^2\right)^2 + \varepsilon_\gamma^2\Gamma(\varepsilon_\gamma)^2} + \frac{0.7\Gamma 4\pi^2 T^2}{E^5}\right], \tag{4}$$

where σ_0 (mb), Γ (MeV), and E (MeV) are the GDR parameters, ε_γ is the γ-ray energy in MeV. The nuclear temperature is defined as: $T = \sqrt{(B_n - \varepsilon_\gamma)/a}$, B_n is the neutron binding energy and a is the Fermi gas level density parameter. The energy-dependent damping width is given by:

$$\Gamma(\varepsilon_\gamma) = \Gamma\frac{\varepsilon_\gamma^2 + 4\pi^2 T^2}{E^2}. \tag{5}$$

This is a modification of a standard Lorentzian proposed by Brink and Axel [9]:

$$f_{SLo}(\varepsilon_\gamma, T) = 8.68 \cdot 10^{-8}(\mathrm{mb}^{-1}\mathrm{MeV}^{-2})\sigma_0\Gamma \times \frac{\varepsilon_\gamma \Gamma^2}{\left(\varepsilon_\gamma^2 - E^2\right)^2 + \varepsilon_\gamma^2\Gamma^2}, \tag{6}$$

For the Oslo analysis, the enhanced GLo (EGLo) is used as defined in RIPL-3 [10]:

$$f_{EGLo}(\varepsilon_\gamma, T) = 8.68 \times 10^{-8}(\mathrm{mb}^{-1}\mathrm{MeV}^{-2})\sigma_0\Gamma \times \left[\frac{\varepsilon_\gamma \Gamma_k(\varepsilon_\gamma, T_f)}{\left(\varepsilon_\gamma^2 - E^2\right)^2 + \varepsilon_\gamma^2\Gamma_k(\varepsilon_\gamma, T_f)^2} + \frac{0.7\Gamma_k(\varepsilon_\gamma = 0, T_f)}{E^3}\right], \tag{7}$$

where the energy-dependent width is defined as:

$$\Gamma_k(\varepsilon_\gamma, T_f) = \mathcal{K}(\varepsilon_\gamma)\frac{\Gamma}{E^2}\left[\varepsilon_\gamma^2 + (2\pi T_f)^2\right] \tag{8}$$

and the empirical function $\mathcal{K}(\varepsilon_\gamma)$ is given by:

$$\mathcal{K}(\varepsilon_\gamma) = \kappa + (1 - \kappa)\frac{\varepsilon_\gamma - \varepsilon_0}{E - \varepsilon_0} \tag{9}$$

with $\varepsilon_0 = 4.5$ MeV and κ given by:

$$\kappa = \begin{cases} 1, & A < 148 \\ 1 + 0.09(A - 148)^2\exp[-0.18\cdot(A - 148)] & A \geqslant 148 \end{cases}. \tag{10}$$

The difference between the GLo and EGLo models for the γSF are shown in Fig. 1 where the red lines indicate the $E1$ component of the strength function. Since the EGLo is

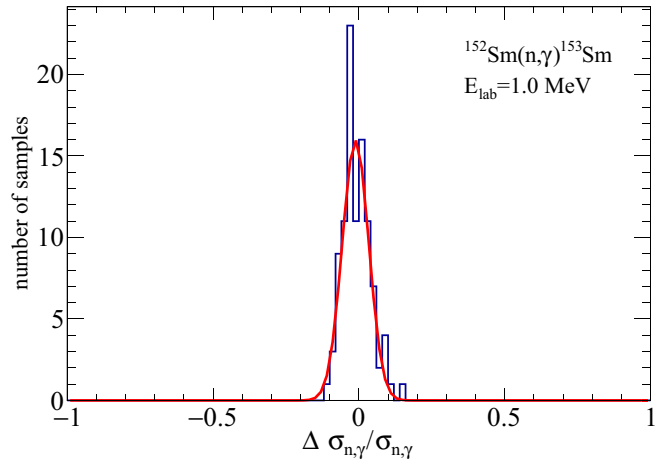

FIG. 2. A sample distribution of the cross section values around the centroid for 10 MeV neutrons in ^{152}Sm (n, γ) ^{153}Sm reaction. Red curve is a Gaussian shape fitted to the distribution in order to determine the σ value.

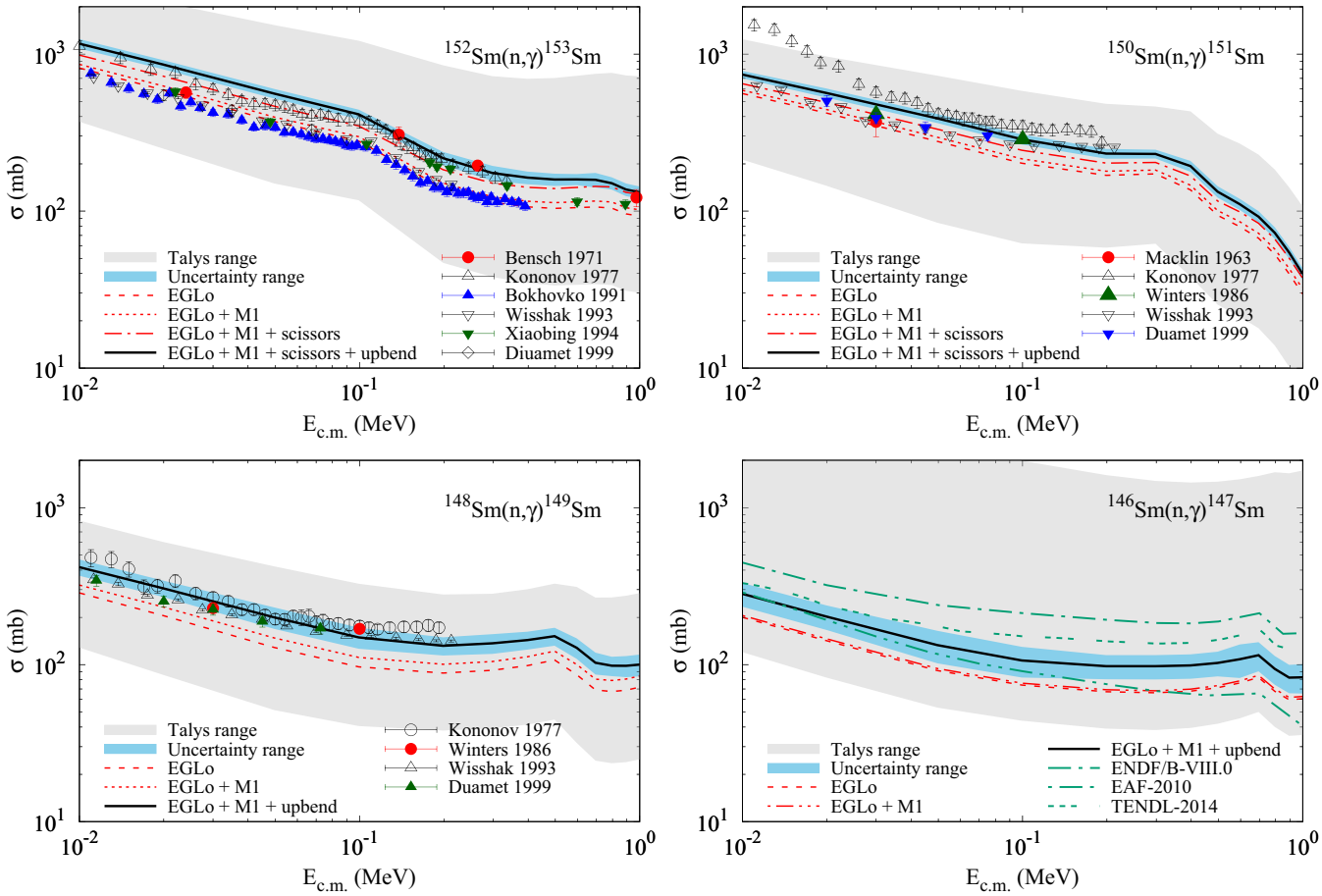

FIG. 3. Neutron capture cross sections obtained in this work. The solid black line is the cross section obtained in this work with a γSF containing $E1$ EGLo, $M1$ spin-flip, scissors mode (if present) and up-bend as defined in Table I. The red lines indicate (n, γ) cross sections obtained for: the EGLo $E1$ function with the TALYS default for $M1$ component (dashed), EGLo with $M1$ as defined in Table I (dotted), and EGLo with spin-flip and scissors mode (dot-dashed). The gray shaded area indicates the range of TALYS predictions with all possible combinations of γSF and LD models, the blue shaded area denotes the 1σ uncertainty obtained from the Monte Carlo analysis. The experimental data were extracted from the EXFOR database [14] and the evaluation data from ENDF [15].

the recommended shape, for the purpose of this work it was implemented into TALYS 1.9 as strength 0.

For the $M1$ component of the γSF, a SLo shape is used throughout the calculations as recommended by RIPL-3 to describe the general shape of the $M1$ strength function. Additionally, for the deformed nuclei, ^{151,153}Sm, a scissors component was added with a SLo shape around 2–3 MeV. For all the compound nuclei, an upbend in the low-energy range of the strength function was added in the form:

$$f_{up} = C\exp(-\eta\varepsilon_\gamma). \tag{11}$$

The parameters for all the components of the γSF were taken from the recent results obtained for the Sm isotopes using the Oslo method [11,12]. A summary of the parameters is given in Table I. The components of the γSF are shown in Fig. 1.

IV. LEVEL DENSITY FUNCTION

In the work of Naqvi *et al.* [12] and Simon *et al.* [11], a constant temperature model (CT) was used to describe the level density. The function was normalized to the number of known levels at low excitation energies and to the level density at the neutron separation energy obtained from neutron resonance data. The list of parameters from Refs. [11,12] is given in Table II.

In order to reproduce the same model for the LD, the constant temperature with Fermi gas model proposed by Gilbert and Cameron [13] was used for this work. The model combines a CT component up to a matching energy value, beyond which a Fermi gas model is used. To ensure that the shape of the LD function in TALYS represented the one extracted from the Oslo method, the matching energy was increased to 17 MeV, beyond the range of the excitation energies covered by the calculations.

V. UNCERTAINTY PROPAGATION

For each calculated cross section, error analysis was performed using Monte Carlo methods. There were total of 14 parameters extracted from the experimental data to describe the γSF and LD. For each parameter an uncertainty as listed in Tables I and II was considered; if the uncertainty was not

TABLE III. (n, γ) reaction cross sections on Sm isotopes investigated in this work.

	Cross section (mb)			
E_{lab} (MeV)	^{152}Sm (n, γ) ^{153}Sm	^{150}Sm (n, γ) ^{151}Sm	^{148}Sm (n, γ) ^{149}Sm	^{146}Sm (n, γ) ^{147}Sm
0.01	1168(82)	742(41)	419(50)	283(49)
0.02	858(57)	566(38)	307(37)	203(36)
0.05	560(39)	390(26)	200(31)	133(31)
0.1	414(29)	287(21)	149(23)	106(24)
0.2	217(21)	232(17)	132(18)	98(17)
0.3	175(19)	231(15)	137(20)	98(17)
0.4	163(15)	193(15)	143(19)	99(17)
0.5	159(14)	133(11)	152(20)	103(18)
0.6	159(13)	110.7(89)	128(19)	108(26)
0.7	158(17)	92.2(78)	103(16)	115(24)
0.8	151(14)	72.6(62)	98(14)	94(20)
0.9	137(13)	54.5(47)	98(15)	83(17)
1.0	132(12)	40.3(34)	100(16)	83(18)
2.0	83.5(85)	56.7(48)	81.4(71)	82(13)
3.0	60.8(62)	95.3(99)	99.0(64)	57.5(65)
4.0	28.9(36)	99(12)	94.7(62)	26.3(25)
5.0	11.9(24)	63.6(82)	64.8(56)	13.4(12)
6.0	4.96(90)	35.5(47)	42.5(45)	7.31(77)
7.0	2.32(21)	20.0(37)	29.8(32)	4.31(47)
8.0	1.39(16)	12.9(29)	23.9(31)	2.95(28)
9.0	1.140(69)	9.3(25)	21.1(31)	2.40(17)
10.0	1.136(52)	7.6(18)	20.0(26)	2.19(12)

given in the original paper, a 5% relative uncertainty was assumed, which is consistent with the uncertainties of other parameters taken into consideration.

The values for all the parameters, except for the centroid of the resonances in the γSF were varied within that uncertainty using a random number generator and assuming a uniform distribution of the parameter values. This was repeated 100 times, and for each set of parameters TALYS calculations were performed. A distribution of cross section values was obtained around the centroid and a Gaussian fit was used to determine its width for each beam energy. An example of the distribution of the relative changes in the cross section at 1.0 MeV in ^{152}Sm (n, γ) ^{153}Sm reaction is shown in Fig. 2. It can be seen that in this case, about 95% of the results with randomized input parameters fall within 20% of the calculated cross section.

VI. NEUTRON CAPTURE CROSS SECTIONS

For each of the four target ^{146,148,150,152}Sm nuclei, several cross-section calculations were performed. First, all possible combinations of γSF and LD models that are available within TALYS were used to extract the range of TALYS predictions for the resulting cross section; the results are shown as a shaded gray region in Fig. 3. Then, calculations were performed using the newly added EGLo strength with the parameters given in Table I and with the default values for the SLo shape of the $M1$ component of the γSF. These calculations are indicated by a red dashed line in all subsets of Fig. 3. Then the $M1$ component was updated to include the parameters listed in Table I (dotted red line). It is clear that with the exception of the ^{152}Sm (n, γ) ^{153}Sm reaction, the EGLo for $E1$ and SLo for $M1$ alone are insufficient to describe the experimental cross sections. The next step of the calculations was to add the scissors mode for the deformed compound nuclei, ^{151,153}Sm; the results are indicated by a red dot-dashed line in Fig. 3. In the final step, the low-energy up-bend with parameters from Table I was added to the γSF. The results are shown as a solid black line with a blue shaded area indicating the 1σ uncertainty calculated using the method described in Sec. V. Fig. 3 shows the results up to 1 MeV for better comparison with the experimental results, full range of the obtained cross-section value for neutron energies up to 10 MeV are listed in Table III. The QRPA calculations of Ref. [16] for ^{148,150,152}Sm (n, γ) ^{149,151,153}Sm also agree well with the present calculations.

A. ^{152}Sm (n, γ) ^{153}Sm cross section

The results of our calculations are in a very good agreement with the data from Refs. [17,18] and overestimate the cross section when compared with the measurements of Refs. [19–22]. The present calculations agree with the results from Refs. [19–22] in the case when up-bend is not included in the γSF.

B. ^{150}Sm (n, γ) ^{151}Sm cross section

The calculated cross sections agree within the experimental uncertainties with those measured by Refs. [17,21,22] at higher energies. At lower energies, $E_{lab} < 0.03$ MeV, the calculations are slightly higher than the results of Refs. [23,24] and significantly diverge from the results of Ref. [17]. Within

TABLE IV. Maxwellian-averaged cross sections for (n, γ) reactions for the thermal energy of 30 keV.

	MACS (mb)			
	^{152}Sm (n, γ) ^{153}Sm	^{150}Sm (n, γ) ^{151}Sm	^{148}Sm (n, γ) ^{149}Sm	^{146}Sm (n, γ) ^{147}Sm
current work	720(80)	490(31)	227(31)	177(27)
Bao *et al.* [28]	473(4)	422(4)	241(2)	–

the experimental uncertainties, an agreement with the data of Refs. [17,21,22] is achieved only when either scissors or both scissors and upbend are included in the calculations.

C. ^{148}Sm (n, γ) ^{149}Sm cross section

In this case, a very good agreement with all experiments found in the literature [17,21,22,24]. At energies above 0.1 MeV, the calculations overlap with the lower range of the experimental uncertainties from Ref. [17]. In this case, it is clear that the up-bend needs to be included in the γSF in order to reproduce the experimental results.

D. ^{146}Sm (n, γ) ^{147}Sm cross section

Since no experimental data for the case of ^{146}Sm (n, γ) ^{147}Sm was found in the literature, the present results are compared with the evaluations from several databases. A relatively large uncertainty in the experimental cross section is obtained for this reaction because of the uncertainty in the upbend parameters and in the D_0 value estimated from systematics in Ref. [12]. The calculated cross section generally follows the trend of the TENDL [25] and ENDF [26] evaluations, but is lower in magnitude by about 25% at the lower energies and by a factor of two at 1 MeV, even after the up-bend was included in the calculations. The EAF [27] evaluation falls below the current results by a factor of two at the higher energies.

VII. DISCUSSION

The results obtained in this work are in a good agreement with with the QRPA calculations performed recently by Filipescu *et al.* [16]. With the exception of ^{152}Sm, the up-bend and scissors (for deformed systems only) are necessary to reproduce the experimental results, provided the $E1$ component of the γ-ray strength function is described as a Lorentzian and a constant-temperature model is assumed for the level density. For the case of ^{152}Sm, the calculations without the up-bend and scissors mode favor the data of Refs. [19–22]. However, the inclusion of the well-established scissors mode in the calculations provides a better agreement with data of Refs. [17,18] and the complete γSF that includes the up-bend reproduces the results of Refs. [17,18].

The procedure described above was also applied to the calculations of the Maxwellian-averaged cross sections (MACS) at the thermal energy of 30 keV for all four reactions. The results were obtained using the built-in functionality of TALYS. The uncertainties in the MACS values were calculated using the Monte Carlo method from Sec. V. The results with 1σ uncertainty are listed in Table IV and are compared with calculations of Bao *et al.* [28]. In the case of ^{148}Sm (n, γ), MACS from the current work is in agreement with that of Ref. [28]. In the case of the deformed systems, ^{152,150}Sm (n, γ), the results from the current work are higher than those of Ref. [28], which is due to the additional low-energy component of the γSF included in the current calculations. Additionally, a MACS of 177(27) mb is obtained for the ^{146}Sm (n, γ) reaction.

ACKNOWLEDGMENTS

This work was supported by the US Department of Energy (NNSA) under Grants No. DE-NA0003780 and No. DE-NA-0003841 (CENTAUR).

[1] F.-K. Thielemann, R. Hirschi, M. Liebendorfer, and R. Diehl, in *Lecture Notes in Physics Vol 812*, edited by R. Diehl (Springer, Berlin, 2011), pp. 153–232.
[2] M. Arnould and S. Goriely, Phys. Rep. **384**, 1 (2003).
[3] J. Escher, L. Ahle, L. Bernstein, J. Burke, J. A. Church, F. Dietrich, C. Forssen, V. Gueorguiev, and R. Hoffman, J. Phys. G: Nucl. Part. Phys. **31**, S1687 (2005).
[4] M. Guttormsen, T. Tveter, L. Bergholt, F. Ingebretsen, and J. Rekstad, Nucl. Instrum. Methods Phys. Res. A **374**, 371 (1996).
[5] A. Spyrou, S. N. Liddick, A. C. Larsen, M. Guttormsen, K. Cooper, A. C. Dombos, D. J. Morrissey, F. Naqvi, G. Perdikakis, S. J. Quinn, T. Renstrøm, J. A. Rodriguez, A. Simon, C. S. Sumithrarachchi, and R. G. T. Zegers, Phys. Rev. Lett. **113**, 232502 (2014).
[6] A. J. Koning, S. Hilaire, and M. C. Duijvestijn, in *Proceedings of the International Conference on Nuclear Data for Science and Technology*, edited by O. Bersillon, F. Gunsing, E. Bauge, R. Jacqmin, and S. Leray (Nice, France, 2008), pp. 211–214.
[7] E. Bauge, J. P. Delaroche, and M. Girod, Phys. Rev. C **63**, 024607 (2001).
[8] J. Kopecky and M. Uhl, Phys. Rev. C **41**, 1941 (1990).
[9] P. Axel, Phys. Rev. **126**, 671 (1962).
[10] R. Capote, M. Herman, P. Obložinsk, P. Young, S. Goriely, T. Belgya, A. Ignatyuk, A. Koning, S. Hilaire, V. Plujko, M. Avrigeanu, O. Bersillon, M. Chadwick, T. Fukahori, Z. Ge, Y. Han, S. Kailas, J. Kopecky, V. Maslov, G. Reffo, M. Sin, E. Soukhovitskii, and P. Talou, Nucl. Data Sheets **110**, 3107 (2009).

[11] A. Simon, M. Guttormsen, A. C. Larsen, C. W. Beausang, P. Humby, J. T. Burke, R. J. Casperson, R. O. Hughes, T. J. Ross, J. M. Allmond, R. Chyzh, M. Dag, J. Koglin, E. McCleskey, M. McCleskey, S. Ota, and A. Saastamoinen, Phys. Rev. C **93**, 034303 (2016).

[12] F. Naqvi, A. Simon, M. Guttormsen, R. Schwengner, S. Frauendorf, C. S. Reingold, J. T. Burke, N. Cooper, R. O. Hughes, S. Ota, and A. Saastamoinen, Phys. Rev. C **99**, 054331 (2019).

[13] A. Gilbert and A. G. W. Cameron, Can. J. Phys. **43**, 1446 (1965).

[14] N. Otuka, E. Dupont, V. Semkova, B. Pritychenko, A. Blokhin, M. Aikawa, S. Babykina, M. Bossant, G. Chen, S. Dunaeva, R. Forrest, T. Fukahori, N. Furutachi, S. Ganesan, Z. Ge, O. Gritzay, M. Herman, S. Hlava, K. Kat, B. Lalremruata, Y. Lee, A. Makinaga, K. Matsumoto, M. Mikhaylyukova, G. Pikulina, V. Pronyaev, A. Saxena, O. Schwerer, S. Simakov, N. Soppera, R. Suzuki, S. Takcs, X. Tao, S. Taova, F. Trknyi, V. Varlamov, J. Wang, S. Yang, V. Zerkin, and Y. Zhuang, Nucl. Data Sheets **120**, 272 (2014).

[15] Evaluated Nuclear Data File (ENDF), https://www-nds.iaea.org/exfor/endf.htm, 2019.

[16] D. M. Filipescu, I. Gheorghe, H. Utsunomiya, S. Goriely, T. Renstrøm, H.-T. Nyhus, O. Tesileanu, T. Glodariu, T. Shima, K. Takahisa, S. Miyamoto, Y.-W. Lui, S. Hilaire, S. Péru, M. Martini, and A. J. Koning, Phys. Rev. C **90**, 064616 (2014).

[17] V. N. Kononov, B. D. Yurlov, E. D. Poletaev, and V. M. Timokhov, Yad. Fiz. **26**, 947 (1977).

[18] L. Xiaobing, X. Yijun, Y. Zhihua, and L. Mantian, Chinese J. Nuclear Physics (Beijing). **16**, 275 (1994).

[19] F. Bensch and H. Ledermann, The activation cross section of several nuclides for neutrons of intermediate energies, Progress Report 105, 1971, report from misc. OECD Countries to EANDC.

[20] M. V. Bokhovko, V. N. Kononov, E. D. Poletaev, N. S. Rabotnov, and V. M. Timokhov, *Conference on Nuclear Data for Science and Technology, Juelich, 1991*, p. 62.

[21] K. Wisshak, K. Guber, F. Voss, F. Kappeler, and G. Reffo, Phys. Rev. C **48**, 1401 (1993).

[22] B. Duamet, M. Igashira, M. Mizumachi, S. Mizuno, J. I. Hori, K. Masuda, and T. Ohsaki, J. Nucl. Sci. Technol. **36**, 865 (1999).

[23] R. L. Macklin, J. H. Gibbons, and T. Inada, Nature (London) **197**, 369 (1963).

[24] R. R. Winters, F. Kappeler, K. Wisshak, A. Mengoni, and G. Reffo, Astrophys. J. **300**, 41 (1986).

[25] A. Koning, D. Rochman, J.-C. Sublet, N. Dzysiuk, M. Fleming, and S. van der Marck, Nucl. Data Sheets **155**, 1 (2019), Special Issue on Nuclear Reaction Data .

[26] M. Chadwick, M. Herman, P. Obloinsk, M. Dunn, Y. Danon, A. Kahler, D. Smith, B. Pritychenko, G. Arbanas, R. Arcilla, R. Brewer, D. Brown, R. Capote, A. Carlson, Y. Cho, H. Derrien, K. Guber, G. Hale, S. Hoblit, S. Holloway, T. Johnson, T. Kawano, B. Kiedrowski, H. Kim, S. Kunieda, N. Larson, L. Leal, J. Lestone, R. Little, E. McCutchan, R. MacFarlane, M. MacInnes, C. Mattoon, R. McKnight, S. Mughabghab, G. Nobre, G. Palmiotti, A. Palumbo, M. Pigni, V. Pronyaev, R. Sayer, A. Sonzogni, N. Summers, P. Talou, I. Thompson, A. Trkov, R. Vogt, S. van der Marck, A. Wallner, M. White, D. Wiarda, and P. Young, Nucl. Data Sheets **112**, 2887 (2011), Special Issue on ENDF/B-VII.1 Library .

[27] EAF-2010, European Activation File, https://www.oecd-nea.org/dbforms/data/eva/evatapes/eaf_2010/, 2019.

[28] Z. Y. Bao, H. Beer, F. Käppeler, F. Voss, K. Wisshak and T. Rauscher, At. Data Nucl. Data Tables **76**, 70 (2000).